Vector Control of DFIG-Based Wind Turbine System

Aanchal Singh S. Vardhan[1,*] and Rakesh Saxena[1]

A R T I C L E I N F O

Article history:
Received: 13 May 2020
Revised: 23 June 2021
Accepted: 9 July 2021

Keywords:
Doubly-fed induction generator
Vector control
MATLAB/Simulink
MPPT
Wind turbine system
Velocity of wind

A B S T R A C T

The paper discusses the vector control of the Doubly-Fed Induction Generator (DFIG)-based wind turbine system. The wind energy has become an important part of power networks as demand for renewable energy has grown. Several national grid codes require comprehensive simulation studies under a variety of operating situations to ensure that the specified model has no detrimental effects on the grid. The DFIGs are now used in the majority of wind farms. The goal of this paper is to gain insight into the DFIG turbine system and create vector management to control reactive and active power exchange independently with the grid. The changes in varied parameters of the system due to wind speed variation are illustrated. In this paper, the DFIG and its numerous parts, its working, characteristics and its limits are also discussed. Then the Maximum Power Point Tracking (MPPT) and additionally the rotary engine profile of the DFIG are focused. This paper describes dynamic equations of the induction machine and then vector control method by developing the equations in d-q reference model and also the active and reactive power control. Finally, the concept is validated in MATLAB/Simulink. There is a tendency to observe the power flow and calculate all the mandatory parameters of the system at synchronous, sub-synchronous and super-synchronous regions.

1. INTRODUCTION

The standard energy supply is restricted and increase pollution to the environment [1-3]. Therefore, a lot of attention and interest are paid to the use of renewable energy (RE) sources equivalent to wind energy, electric cell and solar power and so forth wind energy is the quickest growing and most promising RE source among them because it is economically viable [4-5]. India is the world's third-largest source of electricity and its third-largest consumer. India is one of the countries that produces the most electricity from renewable sources. The Asian nation generates 17% of its overall energy from renewable sources. India's alternative energy generation capacity has grown significantly in recent years. The total installed wind power capacity was 37.669 GW as of the twenty-ninth Gregorian calendar month 2020, making it the fourth highest in the world. The potential for alternative energy is primarily spread through the Southern, Western, and Northern regions. A DFIG is an induction machine within which each the stator coil and rotor is connected to a source, thus the name doubly fed [6-8]. The stator of the DFIG is connected to the grid and the rotor is connected in the back-to-back converters in DFIG based mostly WT system [9-10]. The facility flow through rotor is around 20-30 p.c of the power flow through stator aspect hence the rating of the converters used is low which is one in all the benefits of the DFIG based WT system [11]. The facility flow within the stator side is unidirectional; it continually flows from rotary engine to the grid. Whereas in rotor aspect power flow is bidirectional, power flows from rotary engine to grid in super-synchronous operation and from grid to turbine in sub-synchronous mode [12-14]. One attention-grabbing purpose to notice here is that in sub-synchronous mode the facility absorbed from grid is truly fed back to the grid through stator [15-17].

The organization of the paper is as follows. The Section 2 of the paper deals with the overview of wind turbine power generation and characteristics. The MPPT tracking methodology from the wind with different turbine characteristics is explained in Section 3. The Mathematical modelling of rotor and grid side system and also vector controls of the wind energy system is done using MATLAB Simulink which is explained in Section 4. The results obtained from the Simulink model are described in section 5. The simulation and results are discussed in Section 6. Finally, the main findings are concluded in the Section 7. The paper mainly focuses on modelling and

[1]*Department of Electrical Engineering, Shri G.S. Institute of Technology & Science, Indore (Madhya Pradesh) India*.
**Corresponding author:* Aanchal Singh S. Vardhan, Phone: +917518499096, Email: aanchalvardhan123@gmail.com

Simulation of the wind power generation which is given in details. This makes this paper useful for the researchers to get detailed simulation procedure for their study.

2. AN OVERVIEW OF WIND TURBINE POWER CHARACTERISTICS

A DFIG is an induction motor in which both the stator and rotor is connected to a source, hence the name includes doubly fed. In DFIG based WT system the stator is connected directly to the grid whereas the rotor is connected via back-to-back converters. The power flow through rotor is around 20-30 percent of the power flow through stator side hence the rating of the converters used is low which is one of the advantages of the DFIG based WT system. The power flow in the stator side is unidirectional; it always flows from turbine to the grid. Whereas in rotor side power flow is bidirectional, power flows from turbine to grid in super-synchronous operation and from grid to turbine in sub-synchronous mode. One interesting point to note here is that during sub-synchronous mode the power absorbed from grid is actually fed back to the grid through stator. The power contained in a given volume of a wind is given by

$$P = \frac{1}{2} A v^3 \rho \tag{1}$$

where,

P= Power in a given volume of wind

A= Wind blades swept area

v= Wind velocity

ρ = Air density

Whereas the power obtained by the turbine is given by:

$$P = \frac{1}{2} A v^3 \rho C_p \tag{2}$$

The maximum value of Cp is 0.593 which is called Betz limit. This restricts the maximum value of power we can extract from wind to 59.3 percent of total power contained in a block of wind. Cp is actually a function of β and λ. Where pitch angle = β of the wind blade λ is called the tip-speed ratio of the turbine [18].

$$\lambda = \frac{\omega_m R}{v} \tag{3}$$

where,

ω_m = rotational speed of the turbine

R = Radius of the blades

v = velocity of wind

The rotor torque can be defined as:

$$\tau_m = \frac{P}{\omega_m} = \frac{\rho \Pi R^2 v^3 C_p}{2\omega_m} = \frac{\rho \Pi R^3 v^2 C_t}{2} \tag{4}$$

3. MPPT WITH TURBINE PROFILE

The main aim of any WT system is to get highest power at a selected wind speed. In this paper we'll use the rotary engine profile given by the manufacturer to realize the maximum power extraction. A straightforward graph is given in Figure 1 to know the MPPT [7, 19-20].

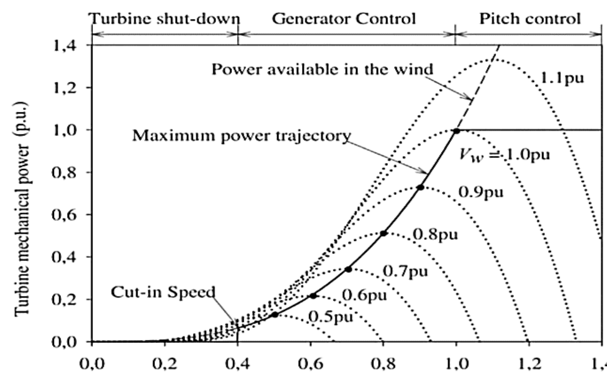

Fig. 1. Maximum power point tracking.

A wind speed sensor measures the wind speed in real time. The P power reference is generated and sent to the generator management system, which contrasts the power reference with the calculated power from the generator to provide management signals for the ability converters, in accordance with the MPPT profile given by the manufacturer. The mechanical power Pm of the engine will be capable of its reference in steady state, by which time the utmost power operation will be accomplished with the help of the regulation of power converters and generators. Since the power losses of the shell and drive-train are ignored in the higher-order analysis, the mechanical power of the generator is equal to the mechanical power generated by the turbine. The details of the rotor side of the DFIG will be discussed in this section [8,21-23].

4. MATHEMATICAL MODELLING

The mathematical modeling of the DFIG system is described in the following sub-sections.

4.1 Converter model

The grid side converter and rotor both are identical. The two-level converter is made up of perfect switches that enable electricity to flow both ways. Signals such as S_{ag}, S_{bg} and S_{cg} are used to control the switches [20].

$$S'_{ag} = \overline{S_{ag}}\,, S'_{bg} = \overline{S_{bg}}\ , S'_{cg} = \overline{S_{cg}} \tag{5}$$

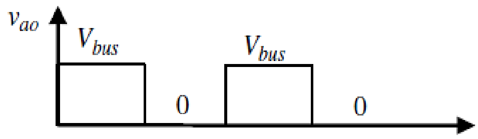

Fig. 2. Two Level Voltage of V_{ao}.

This indicates that both switches cannot conduct at the same time in a specific leg of the converter. It is therefore feasible to produce changing amplitude and frequency AC output voltages fundamental component using various combinations of Sag, Sbg, and Scg. Each phase of this converter may be set to one of two voltage levels. The o/p voltage of converter are attached to grid's 3phase system neutral point on the other hand are quite useful for modelling purposes (n) [16].

$$V_{jn} = V_{jo} - V_{no} \text{ with } j = a, b, c \tag{6}$$

Assuming a 3-phase grid system, require the voltage between the DC bus's neutral (n) and negative points (o).

$$V_{an} + V_{bn} + V_{cn} = 0 \tag{7}$$

Substituting expression

$$V_{no} = \frac{1}{3}(V_{ao} + V_{bo} + V_{co}) \tag{8}$$

Substituting again into Equaton,

$$V_{an} = \frac{2}{3} V_{ao} - \frac{1}{3}(V_{bo} + V_{co}) \tag{9}$$

$$V_{bn} = \frac{2}{3} V_{bo} - \frac{1}{3}(V_{ao} + V_{co}) \tag{10}$$

$$V_{cn} = \frac{2}{3} V_{co} - \frac{1}{3}(V_{ao} + V_{ao}) \tag{11}$$

Table 1. Output voltages of 2 level VSC

S_{ag}	S_{bg}	S_{cg}	V_{ao}	V_{bo}	V_{co}	V_{an}	V_{bn}	V_{cn}
0	0	0	0	0	0	0	0	0
0	0	1	0	0	V_{bus}	$-\frac{V_{bus}}{3}$	$-\frac{V_{bus}}{3}$	$2\frac{V_{bus}}{3}$
0	1	0	0	V_{bus}	0	$-\frac{V_{bus}}{3}$	$2\frac{V_{bus}}{3}$	$-\frac{V_{bus}}{3}$
0	1	1	0	V_{bus}	V_{bus}	$-2\frac{V_{bus}}{3}$	$\frac{V_{bus}}{3}$	$\frac{V_{bus}}{3}$
1	0	0	V_{bus}	0	0	$2\frac{V_{bus}}{3}$	$-\frac{V_{bus}}{3}$	$-\frac{V_{bus}}{3}$
1	0	1	V_{bus}	0	V_{bus}	$\frac{V_{bus}}{3}$	$-2\frac{V_{bus}}{3}$	$\frac{V_{bus}}{3}$
1	1	0	V_{bus}	V_{bus}	0	$\frac{V_{bus}}{3}$	$\frac{V_{bus}}{3}$	$-2\frac{V_{bus}}{3}$
1	1	1	V_{bus}	V_{bus}	V_{bus}	0	0	0

According to the eight permissible switching states of S_{ag}, S_{bg} and S_{cg} there are eight possible output voltage combinations show all these voltage combinations. The output voltages as noted earlier v_{ao}, v_{bo} and v_{co} only two different voltages level that are the bus voltage (V_{bus}) and 0 therefore, this converter is called **"**two- level converter**".** Whereas output phase voltages (v_{an}, v_{bn}, and v_{cn}) of phase a, b, and c take 5 different levels of voltage as: -2V_{bus}/3, -V_{bus}/3, 0, V_{bus}/3 and 2V_{bus}/3 with the help of simple **6-** pulse generator to implement vector control [18].

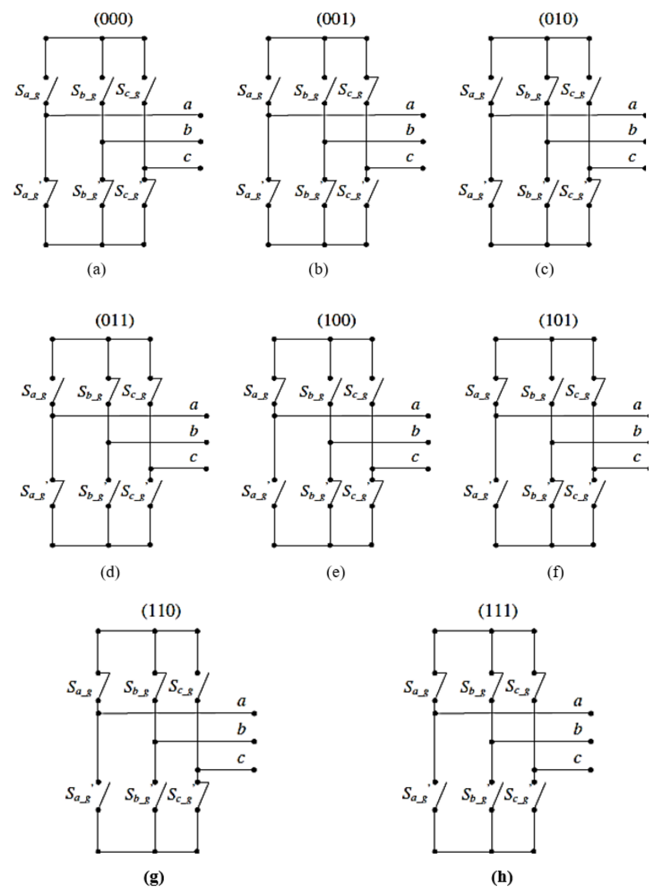

Fig. 3. Eight Different Two-Level VSC Output Voltage Combinations.

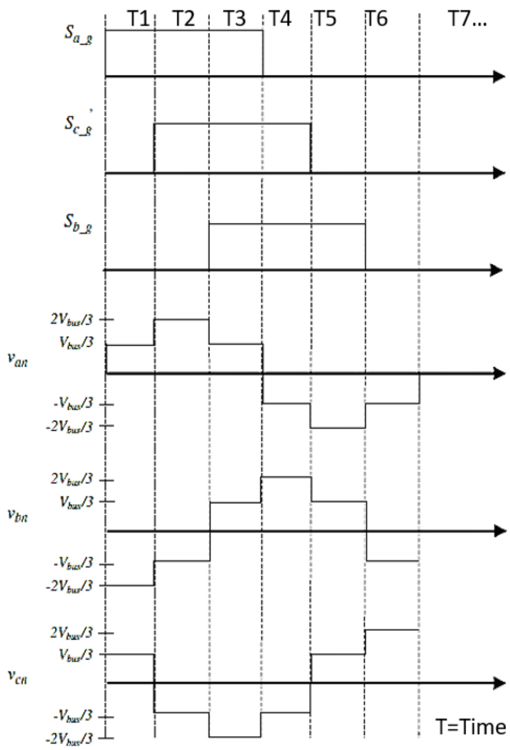

Fig. 4. Two-Level VSC Output Voltage Waveforms with Six Pulse Generation.

4.2 Rotor side system

Dynamic Modelling of Rotor Side System

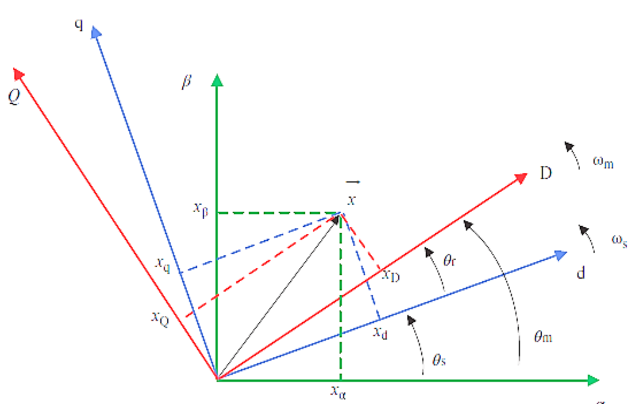

Fig. 5. DFIG Space Vectors Represented in Different Reference Frames.

4.2.1 Two phase (α-β) Modelling: The space vector theory is used to model the α-β dynamics from the mathematical equations obtained using the electric circuit of the machine under steady-state condition.

The α-β is a stationary model D-Q model is a rotor reference frame that rotates at a speed of ω_m the d-q model is synchronous frame that rotates at ω_s. The subscript r, s and a represent that the vector space referred to the rotor, stator and reference axis [20, 23].

$$\overrightarrow{V_s^s} = R_s\overrightarrow{i_s^s} + \frac{d\overrightarrow{\varphi_s^s}}{dt}, \overrightarrow{V_r^r} = R_r\overrightarrow{i_r^r} + \frac{d\overrightarrow{\varphi_r^r}}{dt} \quad (12)$$

$$\overrightarrow{V_s^s} = R_s\overrightarrow{i_s^s} + \frac{d\overrightarrow{\varphi_s^s}}{dt} \Rightarrow \begin{cases} V_{\alpha s} = R_s i_{\alpha s} + \frac{d\overrightarrow{\varphi_{\alpha s}}}{dt} \\ V_{\beta s} = R_s i_{\beta s} + \frac{d\overrightarrow{\varphi_{\beta s}}}{dt} \end{cases} \quad (13)$$

$$\overrightarrow{V_r^s} = R_r\overrightarrow{i_r^s} + \frac{d\overrightarrow{\varphi_r^s}}{dt} - j\omega_m\overrightarrow{\varphi_r^s}$$

$$\Rightarrow \begin{cases} V_{\alpha r} = R_s i_{\alpha r} + \frac{d\omega\alpha_r}{dt} + \omega_m\varphi_{\beta r} \\ V_{\beta r} = R_r i_{\beta r} + \frac{d\omega\beta_r}{dt} - \omega_m\varphi_{\alpha r} \end{cases} \quad (14)$$

Similarly, stator and rotor flux equations are also derived in space vector form instationary frame [48].

$$\overrightarrow{\varphi_s^s} = L_s\overrightarrow{i_s^s} + L_m\overrightarrow{i_r^s} \Rightarrow \begin{cases} \varphi_{\alpha s} = L_s i_{\alpha s} + L_m i_{\alpha s} \\ \varphi_{\beta s} = L_s i_{\beta s} + L_m i_{\beta s} \end{cases} \quad (15)$$

$$\overrightarrow{\varphi_r^s} = L_m\overrightarrow{i_s^s} + L_r\overrightarrow{i_r^s} \Rightarrow \begin{cases} \varphi_{\alpha r} = L_m i_{\alpha s} + L_r i_{\alpha r} \\ \varphi_{\beta r} = L_m i_{\beta s} + L_r i_{\beta r} \end{cases} \quad (16)$$

The magnitudes of the fluxes are sinusoidal in nature whose frequency is s. The stator and rotor, reactive and active power of a system may be estimated as [12].

$$P_s = \frac{3}{2}(V_{\alpha s}i_{\alpha s} + V_{\beta s}i_{\beta s}), P_r = \frac{3}{2}(V_{\alpha r}i_{\alpha r} + V_{\beta r}i_{\beta r}) \quad (17)$$

$$Q_s = \frac{3}{2}(V_{\beta s}i_{\alpha s} + V_{\alpha s}i_{\beta s}), Q_r = \frac{3}{2}(V_{\beta r}i_{\alpha r} + V_{\alpha r}i_{\beta r}) \quad (18)$$

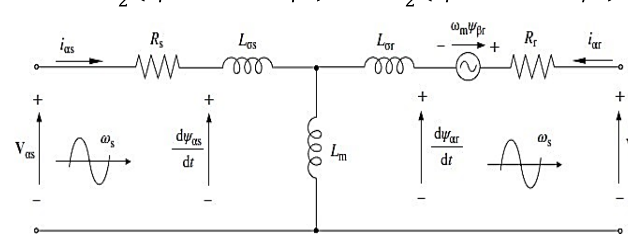

Fig. 6. Reference Frame of the DFIG Model.

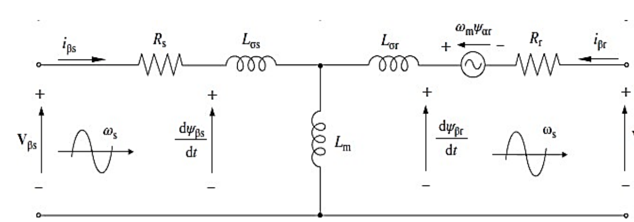

Fig.7. DFIG Reference Frame Model.

The electromagnetic torque can be calculated by

$$T_{em} = \frac{3}{2}pIm\{\overrightarrow{\varphi_r}\,\overrightarrow{i_r^*}\} = \frac{3}{2}p(\varphi_{\beta r}i_{\alpha r} - \varphi_{\alpha r}i_{\beta r}) \quad (19)$$

$$T_{em} = \frac{3}{2}p\frac{L_m}{L_s}Im\{\overrightarrow{\varphi_s}\,\overrightarrow{i_r}\} = \frac{3}{2}\frac{L_m}{\sigma L_r L_s}pIm\{\overrightarrow{\varphi_r^*}\,\overrightarrow{\varphi_s}\} = \frac{3}{2}L_m pIm\{\overrightarrow{i_s}\,\overrightarrow{i_r^*}\} \quad (20)$$

where $\sigma = 1 - L_m^2/L_sL_r$ by adding the mechanical equation

$$T_{em} - T_{load} = J\frac{d\omega_m}{dt} \quad (21)$$

4.2.2 The d-q Modelling: To obtain the d-q model in synchronously rotating frame we multiply the Equations by $e^{-j\theta s}$ and $e^{-j\theta r}$ respectively we get [26]

$$\overrightarrow{V_s^a} = R_s\overrightarrow{i_s^a} + \frac{d\overrightarrow{\varphi_s^a}}{dt} + J\omega_s\overrightarrow{\varphi_s^a} \Rightarrow \begin{cases} V_{ds} = R_s i_{ds} + \frac{d\overrightarrow{\varphi_{ds}}}{dt} - \omega_s\varphi_{qs} \\ V_{qs} = R_s i_{qs} + \frac{d\overrightarrow{\varphi_{qs}}}{dt} + \omega_s\varphi_{ds} \end{cases} \quad (22)$$

$$\overrightarrow{V_r^a} = R_r\overrightarrow{i_r^a} + \frac{d\overrightarrow{\varphi_r^a}}{dt} + j\omega_m\overrightarrow{\varphi_r^a} \Rightarrow \begin{cases} V_{dr} = R_s i_{dr} + \frac{d\omega_{dr}}{dt} - \omega_r\varphi_{qr} \\ V_{qr} = R_r i_{qr} + \frac{d\omega_{qr}}{dt} - \omega_r\varphi_{dr} \end{cases} \quad (23)$$

Similarly, the fluxes

$$\overrightarrow{\varphi_s^a} = L_s\overrightarrow{i_s^a} + L_m\overrightarrow{i_r^a} \Rightarrow \begin{cases} \varphi_{ds} = L_s i_{ds} + L_m i_{dr} \\ \varphi_{qs} = L_s i_{qs} + L_m i_{qr} \end{cases} \quad (24)$$

$$\overrightarrow{\varphi_r^a} = L_m\overrightarrow{i_r^a} + L_r\overrightarrow{i_r^a} \Rightarrow \begin{cases} \varphi_{dr} = L_m i_{ds} + L_r i_{dr} \\ \varphi_{qr} = L_m i_{qs} + L_r i_{qr} \end{cases} \quad (25)$$

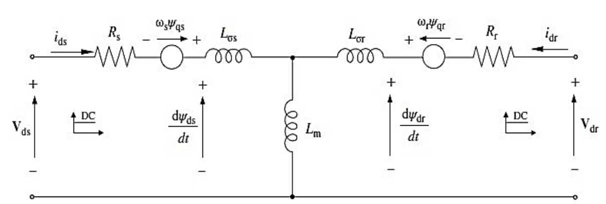

Fig. 8. D Reference Frame Model of the DFIG.

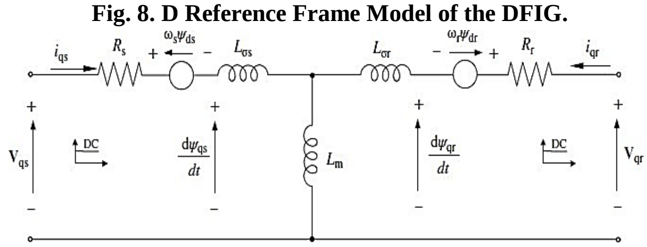

Fig. 9. Q Reference Frame Model of the DFIG.

4.2.3 Vector Control of Rotor Side System

Among different methods of controlling the DFIG, only the vector control is discussed here which is most extensively used control strategy. For easier understanding we will develop it step by step. In the first step we are going to see the current control loops.

4.2.3.1 Rotor Current Control Loop: In the vector control technique of DFIG is operated on synchronously rotating d-q frame, in which the d-axis is in direction with stator flux. Due to this the d-axis of the rotor current is proportional to the stator reactive power whereas the q-axis component is proportional to the torque or stator active power. We will see this later on. We get the rotor voltage as a function of rotor currents and stator flux by substituting Equations. (Note that $\varphi_{qs} = 0$) [9,22].

$$v_{dr} = R_r i_{dr} + \sigma L_r\frac{di_{dr}}{dt} - \omega_t\sigma L_t i_{qr} + \frac{L_m}{L_s}\frac{d|\overrightarrow{\varphi_s}|}{dt} \quad (26)$$

$$v_{qr} = R_r i_{qr} + \sigma L_r\frac{di_{qr}}{dt} + \omega_t\sigma L_t i_{dr} + \frac{L_m}{L_s}\overrightarrow{\varphi_s} \quad (27)$$

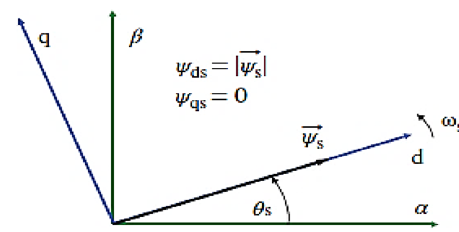

Fig. 10. Synchronous Rotating Reference Frame D-Q Aligned with Stator Flux Space Vector.

From the last two equations we can say that the d and q components of current can be controlled independently by using single regulator for each component. Cross terms in Equations can be included at the output of the regulator and for that we need to estimate the stator flux and ω_r. For transformation of reference frame, we need the angle θ_r. The control is to done in d-q coordinates. To evaluate the θ_r, a basic step locked loop can be used, but we will use a finer approach in our simulation. The current loop, as seen in Figure 11, operates with the currents of rotor side which are referred to the stator, and since the turn ratio is different, we'll take that into account right away [12,23-25].

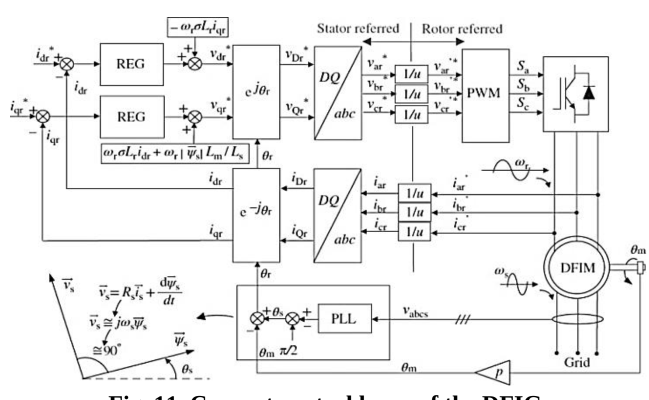

Fig. 11. Current control loops of the DFIG.

4.2.3.2 Speed Control and Power Control: Now that we have developed the current loops we can move on to the power and speed loops. Since the d-axis of the reference frame is aligned to the stator flux the torque equation can be simplified as [14]

$$T_{em}\frac{3}{2}P\frac{L_m}{L_s}(\varphi_{qs}i_{dr} - \varphi_{ds}i_{qr}) = \frac{3}{2}P\frac{L_m}{L_s}|\overrightarrow{\varphi_s}|i_{dr} \quad (28)$$

We can see here that the torque is proportional to the q components of the rotor current; hence we can control the torque by controlling. Similarly we can develop the reactive power of stator part in the d-q model and find i_{qr} that it depends upon the d component of the rotor current.

$$\begin{aligned} Q_s &= \frac{3}{2}\left(V_{qs} i_{ds} - V_{ds} i_{qs}\right) \\ &= -\frac{3}{2}\omega_s \frac{L_m}{L_s} |\overrightarrow{\omega_s}| \left(i_{dr} - \frac{|\overrightarrow{\omega_s}|}{L_m}\right) K_Q = \left(\frac{\overrightarrow{\varphi_s}}{L_m}\right) \end{aligned} \tag{29}$$

Because of the orientation, the authors have chosen to control the active and reactive powers independently. In addition to the current loops discussed earlier we now added power loop as shown in Figure 12. It is possible to control the magnetization of the machine with the Q_s loop. As we know the stator is connected to the power grid directly which has a constant voltage, the stator flux amplitude produced is constant. The stator flux equation reveals that.

$$|\varphi_s| = \varphi_{ds} = L_s i_{ds} + L_m i_{dr} \tag{30}$$

$$\varphi_{qs} = 0 = L_s i_{qs} + L_m i_{qr} \tag{31}$$

The stator flux $|\overrightarrow{\varphi_s}|$ thus must be created by choosing i_{ds} and i_{dr} but these values depend upon the torque and is not in our hands. However, by changing the value of Q_s set we can increase or decrease the stator and rotor currents. For minimizing the rotor currents, the rotor current i_{dr} is set to zero.

4.3 Grid Side System

Now that we have discussed the rotor side system, we now move on to designing the grid side system.

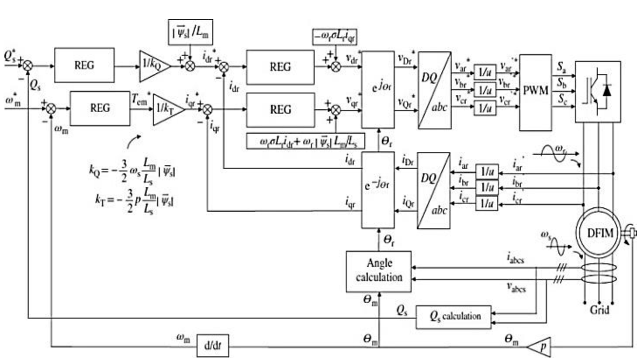

Fig. 12. Complete vector control of the DFIG.

4.3.1 Grid Side Modelling: The equivalent single-phase circuit of grid side system is described in [2,24-26]. The sub-index 'f' is used to label the converter's output AC voltages that are referred to the neutral stage. Hence, the mathematical equations of the electrical machine can be given as:

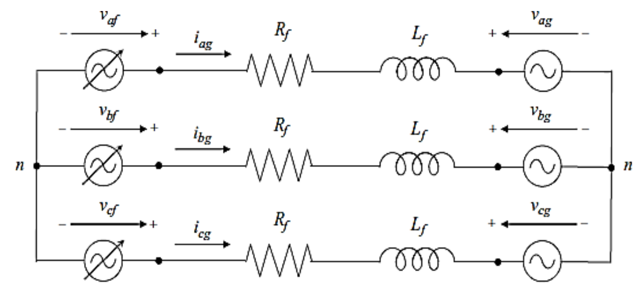

Fig. 13. Simplified Representation of the Three-Phase Grid System.

$$v_{af} = R_f i_{ag} + L_f \frac{di_{ag}}{dt} + v_{ag} \tag{32}$$

$$v_{bf} = R_f i_{bg} + L_f \frac{di_{bg}}{dt} + v_{bg} \tag{33}$$

$$v_{cf} = R_f i_{cg} + L_f \frac{di_{cg}}{dt} + v_{cg} \tag{34}$$

where, L_f is the grid side filter's inductance in H, R_f is the grid side filter's resistive portion (Ω), v_{ag}, v_{bg}, v_{cg} are the voltages on the grid (V), with ω_s electric angular velocity in (rad/s), i_{ag}, i_{bg}, i_{cg} are the currents running from the output of the grid-side converter (A), and v_{af}, v_{bf}, v_{cf} are the converter's output voltages in relation to the load's neutral point n (V). As a result, the first derivative of the currents must be isolated for modelling purposes.

$$\frac{di_{ag}}{dt} = \frac{1}{L_f}\left(v_{af} - R_f i_{ag} - v_{ag}\right) \tag{35}$$

$$\frac{di_{bg}}{dt} = \frac{1}{L_f}\left(v_{bf} - R_f i_{bg} - v_{bg}\right) \tag{36}$$

$$\frac{di_{cg}}{dt} = \frac{1}{L_f}\left(v_{cf} - R_f i_{cg} - v_{cg}\right) \tag{37}$$

4.3.2 α-β Model: It is possible to represent the equations in d-q frame by applying space vector notation to the abc model.

$$V_{af} = R_f i_{ag} + L_f \frac{di_{ag}}{dt} + V_{ag}, V_{\beta f} = R_f i_{\beta g} + L_f \frac{di_{\beta g}}{dt} + V_{\beta g} \tag{38}$$

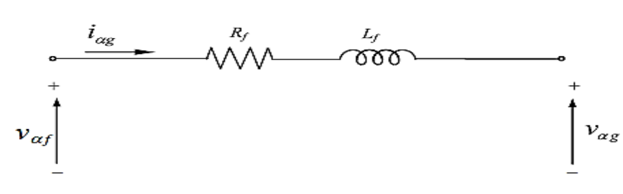

Fig. 14. α Model of the Grid Side.

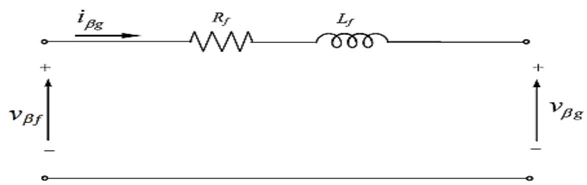

Fig. 15. β Model of the Grid Side.

4.3.3 d-q model: On further simplifying the equation we get

$$v_{df} = R_f i_{dg} + L_f \frac{di_{dg}}{dt} + v_{dg} - \omega L_f i_{qg} \quad (39)$$

$$v_{qf} = R_f i_{qg} + L_f \frac{di_{qg}}{dt} + v_{qg} + \omega L_f i_{dg} \quad (40)$$

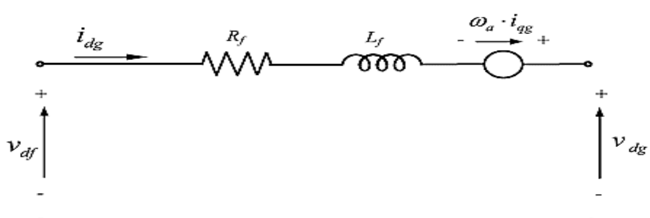

Fig. 16. d Model of the Grid Side.

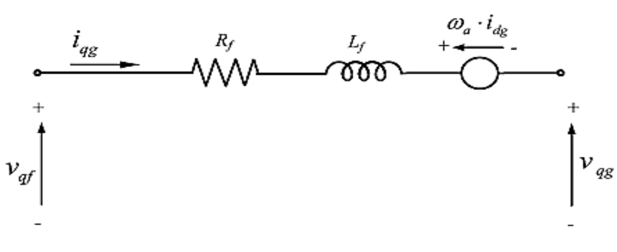

Fig. 17. q Model of the Grid Side.

For further simplification of the machine modelling, the angular speed is considered as the voltage of the grid [27-32]. The direct axis of the d-q frame is directed towards the space vector for fulfilling the space vector control of the machine as given:

$$v_{dg} = \overrightarrow{v_g}, v_{qg} = 0, \omega = \omega_s, \theta_g = \omega_s t \quad (41)$$

Therefore, the expressions become,

$$v_{df} = R_f i_{dg} + L_f \frac{di_{dg}}{dt} + v_{dg} - \omega_s L_f i_{qg} \quad (42)$$

$$v_{qf} = R_f i_{qg} + L_f \frac{di_{qg}}{dt} + v_{qg} + \omega_s L_f i_{dg} \quad (43)$$

The equation of power of the grid can be given in simplified version as:

$$P_g = 1.5 v_{dg} i_{dg}\,,\; Q_g = -\frac{3}{2} v_{dg} i_{qg} \quad (44)$$

It is observed that the reactive and active power exchange with the grid is controllable independently by manipulating i_{dg} and i_{qg} currents.

4.3.4 Grid Side Vector Oriented Control: During this section we have a tendency to be progressing to discuss regarding the grid aspect control system. While not the grid side control system, the DFIG won't work properly. We are going to apply a vector control scheme as shown in Figure 4. The facility generated by the DFIG is partly transmitted from the rotor to the grid side convertor then to the grid. Here we are going to implement a 2 level VSC.

We have a tendency to generate the pulses for the controlled switches two level VSC to regulate the output voltage, that is, the voltage of DC link and additionally to regulate the reactive power ensue the grid. To make sure that power ensue the rotor to the grid aspect convertor then to the grid, the active power got to flow through the dc link, that is made by a capacitor, we've got maintain the dc link voltage to a continuing price with the guarantee that the rotor side and also the grid side converter each has access to the dc link voltage.

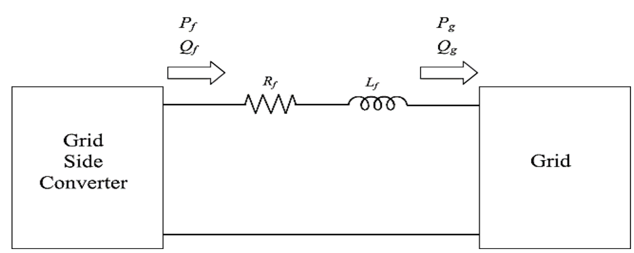

Fig. 18. Power Flow Diagram.

Another variable which will be controlled here is that the reactive power flow. It can take any value relying upon which current we wish to minimize, the present flowing from the mechanical device side or the current flowing from the rotor side. For the grid side management, the magnitudes we'd like to live are the grid side voltage and current at the side of the DC link voltage. We have a tendency to generate pulses for the controlled switches from the references [16].

The d-q voltage references v_{df} *and* v_{qf} is 1st created from the d-q current references, that are i_{dg} *and* i_{qg} from the expression mentioned earlier. This voltage references are then regenerate to fundamentals references mistreatment inverse Clark's and Park's transformation. These fundamentals reference v_{af}, v_{bf} *and* v_{cf} are then fed to modulator that generates pulses consequently to regulate the switches of the grid aspect converter. The latest references i_{dg} *and* i_{qg} are fully decoupled since the space vector of grid voltage and the direct-axis of d-q frame are compatible. The active power P_g is controlled by controllingi_{dg}, and reactive power Q_g is controlled byi_{qg}.

The constant terms needed are deduced from Equations (11) and (12).

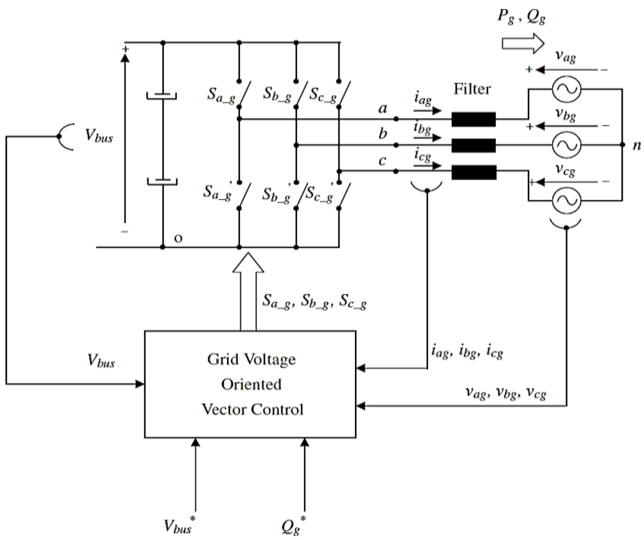

Fig. 19 Grid Side Control.

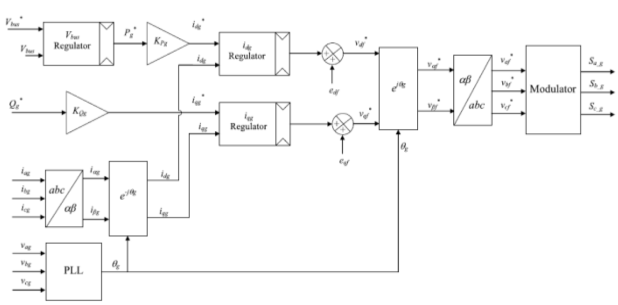

Fig. 20. Grid voltage vector control block diagram.

$$e_{df} = -w_s L_f i_{qg}\,,\ \ e_{qf} = w_s L_f i_{dg} \tag{45}$$

$$K_{P_g} = \frac{1}{\frac{3}{2}v_{dg}},\ K_{Q_g} = \frac{1}{-\frac{3}{2}v_{qg}} \tag{46}$$

The V_{bus} regulator generates the power relation P_g.

5. SIMULATION

In this section we tend to are about to simulate the entire DFIG system in MATLAB and Simulink as shown in Figure 21. We tend to model the wind turbine, rotor aspect system, grid side system and their controls as shown in Figures 6 and 7. Before that we are going to see the various values of the parameters of the machine, constants and alternative pre-defined values that we are going to use within the simulation. We use this power characteristics curve of turbine as shown in Figure 8.

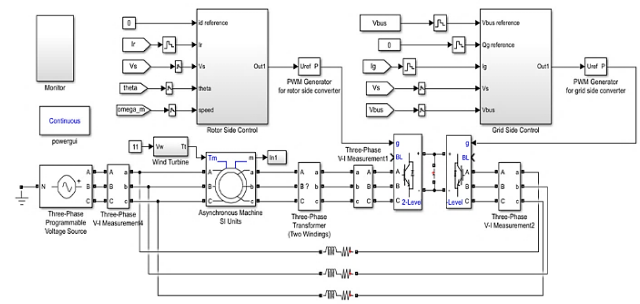

Fig. 21. DFIG in Simulink.

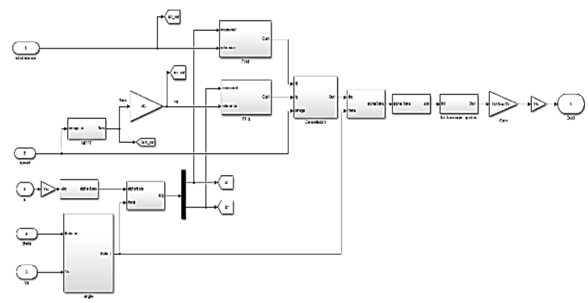

Fig. 22. Rotor Side Control.

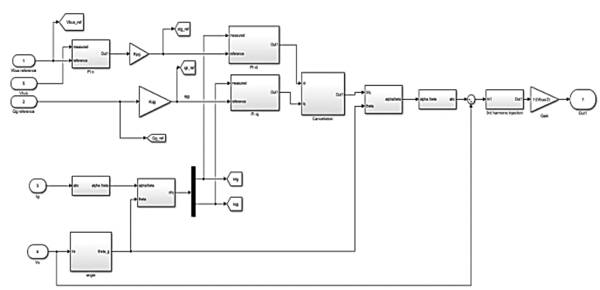

Fig. 23. Grid Side Control.

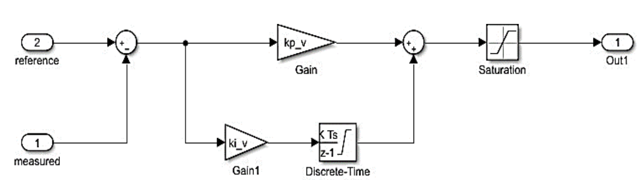

Fig.24 PI Controller for Vbus.

6. SIMULATION RESULTS AND DISCUSSION

In this part, we'll run the simulation to see how the various parameters of the DFIG-based wind turbine system change as the wind speed increases. On the rotor side, the parameters are rotor rpm, torque, $i_{qr}, i_{dr}, v_{dr}, v_{qr}, V_s, I_s$ *and* I_r , and on the grid side,

$V_{bus}, Q_{gref}, i_{dg}, i_{qg}, v_{dg}, v_{qg,}V_s$ *and* i_g .The values of the parameters will be shown first at sub-synchronous speed, then at super-synchronous speed, and finally at synchronous speed. We will keep the reactive power reference at 0 in these two cases. Here the synchronous speed is 1500 RPM.

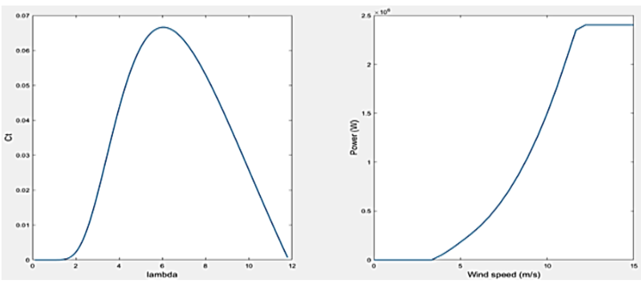

Fig. 25. Lambda vs C_t and Power characteristics graph.

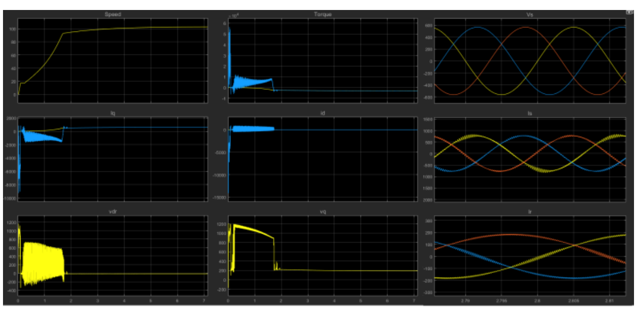

Fig. 26. Parameter values of rotor side at wind speed of 6 m/s (sub-synchronous region).

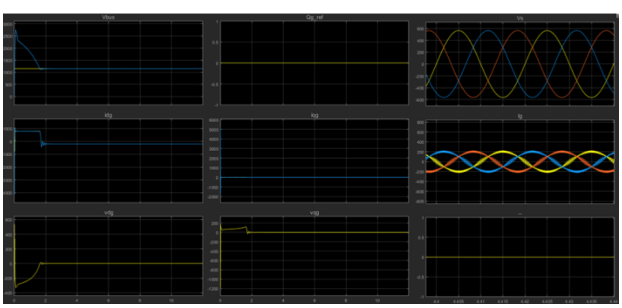

Fig. 27. Parameter values of grid side at wind speed of 6 m/s (sub-synchronous region).

We could observe that the steady state rotor speed is approximately 103 radians per second that is lesser than the synchronous speed. Hence, the machine is operating at sub synchronous region. The steady state torque is 3150 N-m. Hence, the power is calculated as 324260 W, which is close to the value according to the turbine power characteristics we are using. The frequency of $\boldsymbol{i_s}$ current is also close to 50 Hz; hence the frequency is also matched with the grid. The reactive power absorbed by stator for magnetising is discussed later. $\boldsymbol{v_{dg}}$ and $\boldsymbol{i_{dg}}$ is very small (almost close to 0), the active power flow is very minute from grid side to rotor side. Whereas the reactive power is 0 since the value of $\boldsymbol{i_{qg}}$ is 0. This happens because we set the $\boldsymbol{Q_g}$ reference value to 0 to minimize rotor current.

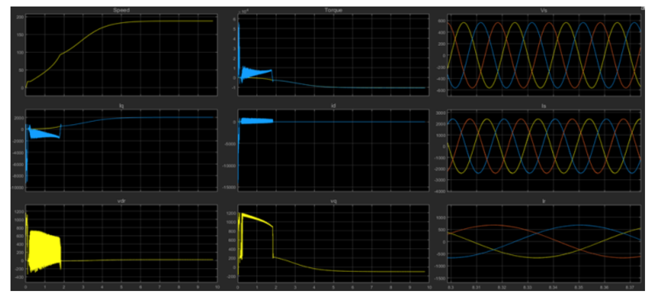

Fig. 28. Parameter values of rotor side at wind speed of 11 m/s (super-synchronous region).

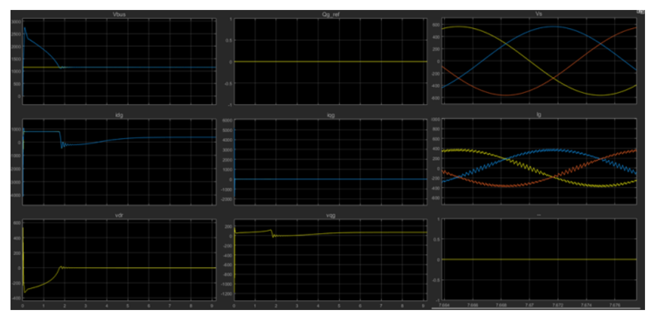

Fig. 29. Parameter values of grid side at wind speed of 11 m/s (super-synchronous region).

We could observe that the steady state rotor speed is approximately 188 radians per second which is more than the synchronous speed; hence the machine is operating at super-synchronous region. The steady state torque is close to 10600 N-m. Hence, the power is calculated as 1992800 W. $\boldsymbol{i_{dg}}$ = 365A and $\boldsymbol{v_{dg}}$ = -2V, the active power transfer from the rotor to the grid is 1095W. Whereas the reactive power is 0 since the value of $\boldsymbol{i_{qg}}$ is 0. This happens because we set the $\boldsymbol{Q_g}$ reference value to 0 to minimize rotor current. The active and reactive power absorbed by filter is found out to be 1.944 W and 12208 VAR.

Since the DFIG is working at synchronous speed the steady state rotor currents are constant values. The active power through the rotor should be 0, and we will verify that now. We know active power through the rotor depends uponi_{dg}. If we look into the steady state value of i_{dg} in above figure, we will see that its value is very close to 0. Hence, the active power is also 0.

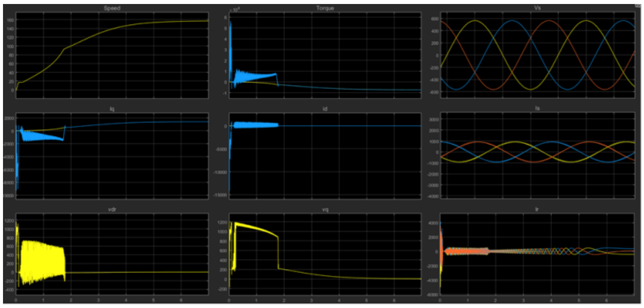

Fig. 30. Parameter values of rotor side at synchronous speed.

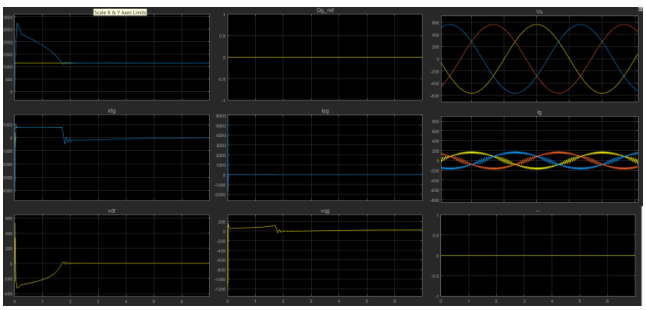

Fig. 31. Parameter values of grid side at synchronous speed

7. CONCLUSION

In this paper DFIG-based wind energy system is studied. During the initial part of the paper, the importance of a wind turbine system is introduced and the wind system is also defined. Later, a DFIG based wind turbine system is modelled theoretically, deriving all the important dynamic modelling equations and based on these equations a DFIG is modelled virtually using software MATLAB and SIMULINK. Finally, the steady state values of all the important parameters are observed in different working conditions, and also calculated the reactive and active powers flowing through both the rotor and stator sides. The simulation results are verified theoretically. It is observed that when the DFIG is working at synchronous speed, the steady state rotor currents are constant values. Also, the active power through the rotor is found to be zero that is obvious.

The future scopes of this paper are as follows:

- This paper will help in modelling the wind energy system for further controlling of any of its part.
- This will also be helpful for further investigation of controller design for wind turbine power generation.

ACKNOWLEDGEMENT

The authors are heartily thankful to the PSRT to bring this research work in its present form. This research work is dedicated to the sweet memories of first author's great grandfather late Shri Ramdas Saket and grandmother late Smt. Terasiya Devi Saket for providing their Aashirvaad, encouragements and constant supports for girl child education in India.

ABBREVIATIONS

DFIGs	Doubly Fed Induction Generators
MPPT	Maximum Power Point Tracking
WT	Wind Turbine
P	Power in a given volume of wind
A	Swept area of the wind blades
v	Wind velocity
ρ	Density of air
β	pitch angle of the wind blade
λ	tip-speed ratio of the turbine
ω_m	rotational speed of the turbine
R	Radius of the blades
v	velocity of wind

REFERENCES

[1] D. P. Kothari, I. J. Nagrath, and R. K. Saket, Modern power system analysis. Tata McGraw-Hill Education, New Delhi, India, 2021.

[2] Om Prakash Bharti, R.K. Saket and S.K. Nagar, "Reliability assessment and performance analysis of DFIG-based WT for wind energy conversion system", *International Journal of Reliability and safety*, Vol.13, No.4, 2019.

[3] L. Varshney and R.K. Saket, "Reliability evaluation of SEIG rotor core magnetization with minimum capacitive excitation for unregulated renewable energy applications in remote areas," Ain Shams Engineering Journal, vol. 5, no. 3, pp. 751–757, 2014.

[4] R.C. Bansal, "Three-phase self-excited induction generators: an overview," IEEE transactions on energy conversion, vol. 20, no. 2, pp. 292–299, 2005.

[5] R.K. Saket, "Design aspects and probabilistic approach for generation reliability evaluation of mww based micro-hydro power plant," Renewable and Sustainable Energy Reviews, vol. 28, pp. 917–929, 2013.

[6] A. Chen, D. Xie, D. Zhang, C. Gu, and K. Wang, "Pi parameter tuning of converters for sub-synchronous interactions existing in grid-connected DFIG wind turbines," IEEE Transactions on Power Electronics, vol. 34, no. 7, pp. 6345–6355, 2018.

[7] S. Khateri-abri, S. Tohidi, and N. Rostami, "Improved direct power control of DFIG wind turbine by using a fuzzy logic controller," IEEE 10th International Power Electronics,

Drive Systems and Technologies Conference (PEDSTC), 2019, pp. 458–463.

[8] H.-S. KO, G.-G. Yoon, N.-H. Kyung, and W.-P. Hong, “Modelling and control of DFIG-based variable-speed wind-turbine,” Electric Power Systems Research, vol. 78, no. 11, pp. 1841–1849, 2008.

[9] O.P. Bharti, R.K. Saket, and S.K. Nagar, “Controller design of DFIG-based WT by using de-optimization techniques,” IEEE SICE International Symposium on Control Systems (SICE ISCS), Japan, pp. 128–135, 2018.

[10] M. Mohseni, S. Islam, and M. A. Masoum, “Using equidistant vector-based hysteresis current regulators in DFIG wind generation systems,” Electric Power Systems Research, vol. 81, no. 5, pp. 1151–1160, 2011.

[11] Kumari Sarita, Sachin Kumar, Aanchal Singh S. Vardhan, Rajvikram Madurai Elavarasan, R.K. Saket, G.M. Shafiullah, Eklas Hossain, “Power enhancement with grid stabilization of renewable energy-based generation system using UPQC-FLC-EVA technique,” IEEE Access, Vol. 8, Pages: 207443-207464 2020.

[12] Santos Martin, D., et al., “Direct power control applied to doubly fed induction generator under unbalanced grid voltage conditions”, IEEE Trans. Power Electron. **23** (5), 2328– 2336, 2008.

[13] Om Prakash Bharti, R.K. Saket, S.K. Nagar, “Controller design for doubly fed induction generator using particle swarm optimization technique”, Renewable Energy, Volume 114, Part B, Pages 1394-1406, December 2017.

[14] Om Prakash Bharti, R.K. Saket, S.K. Nagar, “Controller design of DFIG based wind turbine by using evolutionary soft computational techniques”, Engineering, Technology & Applied Science Research, Vol. 7, No.3 Pages:1732-1736, 2017.

[15] F. Yao, R.C. Bansal, Z.Y. Dong, R.K. Saket, J.S. Shakya, “Wind Energy Resources: Theory, Design, and Applications”, Handbook of Renewable Energy Technology, World Scientific Publishing House, Singapore, 2011.

[16] M. Tazil, V. Kumar, R.C. Bansal, S. Kong, Z.Y. Dong, W. Freitas, H.D. Mathur, “Three-phase doubly fed induction generators: an overview”. IET Electric Power Applications, Vol. 4, pp. 75–89, 2010.

[17] O.P. Bharti, R.K. Saket, S.K. Nagar, “Controller Design for DFIG Driven by Variable Speed Wind Turbine Using Static Output Feedback Technique”, Engineering, Technology & Applied Science Research, Vol. 6, No. 4, pp-1056-1061, 2016.

[18] O.P. Bharti, R.K. Saket, S.K. Nagar, “Reliability Analysis of DFIG Based Wind Energy Conversion System”, ICRET-2017, Thammasat University, Bangkok, Thailand, pp: 313-317, 2017.

[19] habib0264 BENBOUHENNI, Habib. "Application of STA Methods and Modified SVM Strategy in Direct Vector Control System of ASG Integrated to Dual-Rotor Wind Power: Simulation Studies." International Journal of Smart Grid-ijSmartGrid 5, no. 1 (2021): 63-73.

[20] Benbouhenni, Habib. "Comparison study between seven-level SVPWM and two-level SVPWM strategy in direct vector control of a DFIG-based wind energy conversion systems." International Journal of Applied Power Engineering (IJAPE) 9, no. 1 (2020): 12-21.

[21] Bose, Sourav, and S. P. Singh. "Sensor-less Vector Control of DFIG Based Micro Wind Energy Conversion System." In *2020 IEEE* International Conference on Power Electronics, Smart Grid and Renewable Energy (PESGRE2020), pp. 1-6. IEEE, 2020.

[22] Velpula, Srikanth, and Thirumalaivasan Rajaram. "A simple approach to modelling and control of DFIG-based WECS in network reference frame." International Journal of Ambient Energy (2020): 1-11.

[23] Dbaghi, Yahya, Sadik Farhat, Mohamed Mediouni, Hassan Essakhi, and Aicha Elmoudden. "Indirect power control of DFIG based on wind turbine operating in MPPT using backstepping approach." International Journal of Electrical & Computer Engineering (2088-8708) 11, no. 3 (2021).

[24] Jenkal, H., B. Bossoufi, A. Boulezhar, A. Lilane, and S. Hariss. "Vector control of a Doubly Fed Induction Generator wind turbine." Materials Today: Proceedings 30 (2020): 976-980.

[25] Sachin Kumar, Kumari Sarita, R.K. Saket, D.K. Dheer, R.C. Bansal, Saad Mekhilef (2021), “Reliability Assessment for DFIG-based WECS Considering the Impact of 3-phase fault and Lightning Impulse Voltage”, International Transactions on Electrical Energy Systems (WoS & SCIE), In press, 2021.

[26] Om Prakash Bharti, Kumari Sarita, Aanchal Singh S. Vardhan, Akanksha Singh S. Vardhan, R.K. Saket (2021), “Controller Design for DFIG-based WT Using Gravitational Search Algorithm for wind power generation”, IET Renewable Power Generation (UK), In Press, 2021.

[27] R.C. Bansal, A.F. Zobaa and R.K. Saket (2005), “Some issues related to power generation using wind energy conversion system: An Overview”, International Journal of Emerging Electric Power System, volume: 3, Issue: 2, pp: 01-19, October 26, 2005, Article 1070, Berkeley, Canada 94705, Web Site: http://www.bepress.com.

[28] Ahmed M. Atallah, Almoataz Y. Abdelaziz, Mohamed Ali, R.K. Saket, O.P. Bharti (2015) “Reliability assessment and economic evaluation of offshore wind farm using stochastic probability”, Advances in Intelligent Systems and Computing, Publisher: Springer Nature, ISSN: 2194-5357, Springer Verlag, Germany. https://www.scopus.com/source.

[29] Sachin Kumar, Kumari Sarita, R.K. Saket, D.K. Dheer, R.C. Bansal, Saad Mekhilef (2021), “Reliability Assessment for DFIG-based WECS Considering the Impact of 3-phase fault and Lightning Impulse Voltage”, International Transactions on Electrical Energy Systems, volume 31, issue 8, e12952, 2021.

[30] Ahmed M. Atallah, Almoataz Y. Abdelaziz, Mohamed Ali, R.K. Saket and Anand Kumar K.S. (2014), “Cable Laying Precautions in Offshore Wind Farms with Reactive Power Compensation”, International Conference on Power Electronics and Renewable Energy Systems, Proceeding published by LNEE series of SPRINGER, Rajalakshmi Engineering College, Chennai, India. April 24-26, 2014, pp: 01-08. Site: http://www.spinger.com

[31] Rishikesh Choudhary and R.K. Saket (2015), "A Critical Review on the Self-Excitation Process and Steady State Analysis of an SEIG Driven by Wind Turbine", Renewable and Sustainable Energy Reviews, Volume: 47, July 2015, pp: 344-353. Web-site: http://www.sciencedirect.com/rser.

[32] Lokesh Varshney and R.K. Saket (2014), “Reliability Evaluation of SEIG rotor core magnetization with minimum capacitive excitation for unregulated renewable energy applications in remote areas”, Ain Shams Engineering Journal, Elsevier, September 2014; volume: 5, issue: 3, pp: 751-757. Web-site: http://www.sciencedirect.com/asej.